

Efficient Memristive Spiking Neural Networks Architecture with Supervised In-Situ STDP Method

Santlal Prajapati *, Susmita Sur-Kolay*, and Soumyadeep Dutta†

Abstract—Memristor-based Spiking Neural Networks (SNNs) with temporal spike encoding enable ultra-low-energy computation, making them ideal for battery-powered intelligent devices. This paper presents a circuit-level memristive spiking neural network (SNN) architecture trained using a proposed novel supervised in-situ learning algorithm inspired by spike-timing-dependent plasticity (STDP). The proposed architecture efficiently implements lateral inhibition and the refractory period, eliminating the need for external microcontrollers or ancillary control hardware. All synapses of the winning neurons are updated in parallel, enhancing training efficiency. The modular design ensures scalability with respect to input data dimensions and output class count. The SNN is evaluated in LTspice for pattern recognition (using 5×3 binary images) and classification tasks using the Iris and Breast Cancer Wisconsin (BCW) datasets. During testing, the system achieved perfect pattern recognition and high classification accuracies of 99.11% (Iris) and 97.9% (BCW). Additionally, it has demonstrated robustness, maintaining an average recognition rate of 93.4% under 20% input noise. The impact of stuck-at-conductance faults and memristor device variations was also analyzed.

Index Terms—Memristor, Spiking neural network, Supervised in-situ training, Lateral inhibition, Refractory period.

I. INTRODUCTION

The primary focus of contemporary software systems is on Artificial Intelligence (AI) tasks [1]. A fast and power-efficient hardware platform is essential for implementing Artificial Neural Networks (ANNs), the primary technologies that enable AI tasks. Adopting biologically plausible information processing primitives, such as spiking neural networks (SNN), is recommended as a power-efficient platform [2]. SNNs are more power-efficient than ANNs due to their spike-driven sparse computation feature. These third-generation neural networks [3] exhibit event-driven computation, diverse coding mechanisms, and rich neurodynamic characteristics in both space and time [2].

In order to achieve brain-inspired efficiency, SNNs require a hardware architecture that supports synaptic plasticity, high parallelism, high-density integration, and low power-driven devices. The nano-sized, nonlinear memristor devices, first fabricated in HP Labs in 2008 [13], are promising candidates for SNN hardware design. Memristors [14] are passive, nonlinear circuit elements with variable nonvolatile resistance

states, similar to biological synapses. They are compatible with CMOS technology [15]. In SNN circuit implementations, memristors enable the co-location of computation and memory [16], thus alleviating the memory bottleneck problem [17], a major impediment to data-intensive ANN workloads.

Existing research [4]–[7], [11], [12], [18]–[24] has explored in-situ trainable circuit implementations of memristive SNNs for high processing speed, low power dissipation, and high parallelism. In-situ training is performed on neuromorphic hardware itself [25]. However, related works [18]–[20], [22] require additional control units like micro-controllers or FPGAs. Although some memristive SNNs with in-situ training mechanisms eliminate external control units, their hardware complexity remains high [4]–[7]. In a memristive SNN architecture, the simplicity of the artificial synapse circuit is crucial for scalability. In [4], the artificial synapse circuit using commercial ICs and discrete semiconductor components is complex. Similarly, the synapse update circuit in [6] uses commercial ICs, making the solution less economical.

The winner-takes-all (WTA) mechanism, where only one neuron spikes while the others are laterally inhibited, is attractive for low-power neuromorphic computation applications. While WTA has been implemented [5], [23] using a separate memristive crossbar array and mixed-signal peripheral circuits [5], we propose a complete analog approach without any extra memristive crossbar for this strategy. Furthermore, the WTA architectures proposed in [6], [7] have post-synaptic neurons connected in a mesh topology, hindering scalability. We propose a more scalable and hardware-efficient alternative.

In the literature [4]–[7], researchers have focused on pattern recognition tasks, while others [8], [9] have addressed classification problems using memristor-based SNNs. For instance, Sboev et al. [8] proposed a mathematical model of memristive SNNs for classification tasks, whereas Jiang et al. [9] suggested a hardware architecture of memristive SNNs with a hidden layer, implementing WTA and refractory period as computational primitives. The hardware complexity of Jiang's memristive SNN architecture [9] is a concern due to its multi-synaptic model and the use of commercial ICs. Our memristive SNN architecture is simpler at the circuit-level, has no hidden layer, and uses 1T1M (one transistor, one memristor) synapse.

Our architecture can be used for pattern recognition as well as classification problems. Identification of a structure in an image input is termed as pattern recognition [4]–[7], whereas assigning of input sample, which may not be an image, to one of the several predefined categories or classes [8], [9], [12] is called classification problem. For classification, inputs are preprocessed with the Gaussian receptive field method [8],

S. Prajapati, School of Engineering, Sister Nivedita University, DG 1/2 New Town, Action Area 1, Kolkata - 700156, E-mail: santlal.p@snuniv.ac.in

S. Sur-Kolay, Advanced Computing and Microelectronics Unit, Indian Statistical Institute, Kolkata-700108, India, E-mail: surkolay@gmail.com

S. Dutta, Research Scientist, in EdPi, Noida, Basi Bahuddin Nagar, Uttar Pradesh 201304 E mail: soumyadeepd@edpi.ai

TABLE I
QUALITATIVE COMPARISON WITH PREVIOUS WORKS

Papers	Synapse	Learning algorithm	The way to update the memristive synapses of MC	WTA	Refractory period	Image recognition and # training Samples to get same accuracy	Major hardware components affecting power and area	Problems solved
[4]	2 Op, 4T, 1M	STDP Unsupervised	Parallel	No	No	No, —	Two Op per synapse	Pattern recognition
[5]	1T1M	Hebbian Unsupervised at first layer and supervised at second layer	Parallel	Yes	Yes	Ten 6x5 digits, —	Flip-flops, AND gates, and buffer in neurons	Pattern recognition
[6]	1M	Unsupervised STDP	Parallel	Yes	No	Four 5x3 digits, 3000	$(m-1)$ NMOS T, two OP and Two 74121 ICs (monostable multivibrators) per post-neuron	Pattern recognition
[7]	1M 1 Dual Switch	Hebbian Unsupervised	Parallel	Yes	No	Four 5x3 letters, 400	One OP, $(m-1)$ PMOS T per post-neuron	Pattern recognition
[8]	—	Supervised STDP	Parallel (Theoretically)	Yes	Yes	No, —	Mathematical model	Classification
[9]	2M	SpikeProp [10]	Parallel	No	No	No, —	555-timer and three C per neuron. Delay circuit per synapse multiple synapses between pre- and post-neurons	Classification
[11]	4M2R	Unsupervised STDP	Parallel	No	No	3×3 patterns	Synapses and subtractors STDP circuits and trace modules	pattern recognitions
[12]	fully complex CMOS synapse	On-chip STDP (unsupervised)	Parallel	No	Yes	XOR and MNIST	CMOS-based memristor emulators, Spike Processing Circuitry	classification
This work	1T1M	Supervised STDP	Parallel	Yes	Yes	four 5x3 digits, 100 7x3 digits	Three OPs per post-neuron One comparator per pre-neuron	Pattern recognition and Classification

Op: Operational amplifier, T: Transistor, M: Memristor, R: Resistor, C: Capacitor, WTA: Winner-Takes-All, m : Number of post-neurons, MC: Memristive Crossbar

which increases robustness against faulty memristors. Inputs are encoded into spikes using the temporal spike encoding method [8]. Temporal encoding and sparse synapse updating (only the winner's synapses are updated in parallel) make the proposed SNN more time-energy-efficient compared with one having rate encoding of spikes [26].

Table I provides a qualitative comparison with similar previous works solving pattern recognition and classification problems, highlighting the advantages of the proposed approach in terms of hardware complexity and statistical efficiency.

The complete and simple, hardware and training latency efficient, in-situ trainable, and external microcontroller free memristive SNN architecture that solves pattern recognition and classification problems are the motivations of this work. In this work, we contribute the following:

- a complete circuit-level architecture of a trainable and scalable memristive SNN that does not require any external control units such as a micro-controller or an FPGA,
- a supervised in-situ STDP training algorithm is proposed,
- design of peripheral/control circuits to accomplish training, emulate WTA strategy and refractory period while achieving high accuracy and F1-score,
- a thorough study of the effects of faulty memristors and device variations in parameters such as R_{on} , R_{off} , and the threshold voltage of a memristor on the performance of the SNN,
- an analysis of robustness against noisy patterns in the memristive SNN.

In the rest of this article, Section II explains the spiking neural network model, memristor, and memristive crossbar, and data pre-processing for classification by SNN. Section III gives the overview and layout of the proposed memristive SNN architecture. It also details the major components of the architecture. Section IV discusses the supervised in-situ STDP training algorithm. Section V presents the simulation and results with concluding remarks in Section VI.

II. PRELIMINARIES

A. Spiking Neural Networks

In a spiking neuronal network, a spike or an action potential is a short electrical pulse used for inter-neuron communication [27]. Each spiking neuron has a membrane potential that increases upon receiving a spike and gradually decreases afterward. When there are no input spikes then it stays at resting potential. A neuron fires a spike when its membrane potential crosses the threshold potential and afterward, it goes below resting potential [27]. Once a neuron fires the spike, it waits for some time, called the refractory period, to fire again. In a layer of neurons, when a neuron fires it inhibits others to fire. This is called lateral inhibition which makes the spike communication sparse.

The spiking neural network (SNN) model employed in this work is shown in Fig. 1. It is simple and has no hidden layers performing both classification and pattern recognition tasks. The working process of it is as follows —

- The input feature vector $\mathbf{x} = [x_1, x_2, \dots, x_n]$, at the input layer, are encoded into spikes, specifically called pre-synaptic spikes or here *pre_spikes*, using temporal spike encoding method explained in Section III-A.
- These *pre_spikes* travel via weighted synapses to neurons at the output layer called post-synaptic neurons or here *post_neurons* is denoted as LIF_1 to LIF_m . The synapse $s_{m,1}$ denotes the connection between *post_neuron_m* and *pre_neuron₁* (or *pre_spike₁*) with synaptic weight $w_{m,1}$.
- The post-neurons are competitive, they compete amongst themselves to fire first and laterally inhibit others using the inhibition module.
- The neuron that spikes first sends its *post_spike* to the inhibition module and in response to that inhibition module sends inhibition pulse signal v_{inh} to all LIFs to prevent their firings.
- The neuron that spikes first is called winner and this process is called winner-takes-all (WTA). The v_{inh} plays a

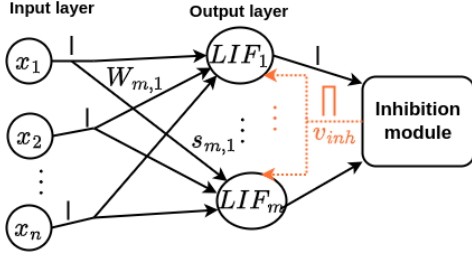


Fig. 1. Spiking neural network model. The features at the input layer are encoded into spikes and via synapses they travel to post-synaptic neurons at the output layer. The m^{th} post-synaptic neuron is denoted as LIF_m . The inhibition module implements WTA and refractory period with generated inhibition signal v_{inh} .

vital role in implementing the refractory period, discussed in Section III-E.

For a dataset, if there are n features and m classes then there are n *pre_spikes*, m *post_neurons*, and $n \times m$ weighted synaptic connections. The SNN models are trained with the proposed supervised algorithms based on STDP [28] (detailed in Section IV).

B. Memristor model and memristive crossbar

Memristors, due to their nano-scale size and variable non-volatile conductance states, are the most suitable devices to implement artificial synapses and emulate synaptic plasticity in neuromorphic systems. The spice model of voltage-controlled threshold memristor proposed by Yang *et al.* [29] is chosen to design a synapse in this work. The mathematical expressions of memristors are:

$$\begin{cases} v(t) = R(t)i(t) \\ R(t) = R_{on} \frac{w(t)}{D} + R_{off}(1 - \frac{w(t)}{D}) \end{cases} \quad (1)$$

where, $v(t)$, $i(t)$, $R(t)$, D , R_{on} , R_{off} , and $w(t)$ are voltage, current, memristance of memristor, width of memristive device, minimum memristance, maximum memristance, and width of doped region in the memristive device respectively. The dynamics of $w(t)$ is as follows:

$$\frac{dw(t)}{dt} = \begin{cases} \mu_v \frac{R_{on}}{D} \frac{i_{off}}{i(t)-i_0} f(w(t)), & v(t) > V_{T+} > 0 \\ 0, & V_{T-} \leq v(t) \leq V_{T+} \\ \mu_v \frac{R_{on}}{D} \frac{i(v)}{i_{on}} f(w(t)), & v(t) < V_{T-} < 0 \end{cases} \quad (2)$$

where, μ_v , $f(w(t))$, V_{T+} , and V_{T-} are average ion mobility, window function, and positive & negative threshold voltages respectively. The i_{on} , i_{off} , and i_0 are fitting parameters. The window function $f(\cdot)$ is given by:

$$f(w(t)) = 1 - \left(\frac{2w(t)}{D} - 1 \right)^{2p} \quad (3)$$

Where p is a positive constant. The parameters' values used in this work are listed in Table II which matches the characteristics of PCMO-based practical memristor device [30], [31]. A positive voltage across the memristor, greater than the positive threshold, increases its conductance and vice versa [29].

The structure where memristors are organized in a 2D array is called memristive crossbar (MC) [32]. On MC, memristors

TABLE II
THE PARAMETER VALUES USED IN THE SPICE MEMRISTOR MODEL.

Spice model parameters	D(nm)	$\mu_v(m^2s^{-1}\Omega^{-1})$	$R_{on}(\Omega)$	$R_{off}(\Omega)$	$V_{T-}(V)$	$V_{T+}(V)$	$i_{on}(A)$	$i_{off}(A)$	$i_0(A)$
Values	3	$3.2e-15$	$1e6$	$6e7$	-2.4	1.2	1	$1.4e-14$	$3e-8$

are placed alone (1M type, 2M type, 2M1M types) [6], [33], [34] or with transistors [32], [35] (1T1M or 2T1M types, etc). The 1T1M type crossbar is shown in the green dashed box of Fig. 2(a). It is used to perform matrix-vector multiplication when MC is considered a matrix of memristors' conductance and the vector is voltages to the rows of MC [36], [37].

C. Data Pre-processing

For classification problems, the input features are pre-processed by min-max scale followed by Gaussian receptive field methods [38]. The Gaussian receptive field method expands an input vector \mathbf{x} (originally n_1 -dimensional) to a higher-dimensional space (n_1, n_2) where n_2 is number of receptive fields. Each element x_i of \mathbf{x} is expanded to n_2 components [8], [38]. Only for classification simulations, we perform Gaussian receptive field pre-processing with $n_2 = 3$ but not for pattern recognition. After pre-processing it is assumed that the minimum and maximum values of each feature are 0 and T respectively. This method has been widely used in SNN-based models [8], [38]–[41].

III. MEMRISTIVE SNN ARCHITECTURE

Fig. 2(a) illustrates the overview of the proposed memristive SNN. The main components include a temporal spike encoder, dual switches, a memristive crossbar (MC), Leaky Integrate-and-Fire (LIF) neurons, and various proposed control modules such as the lateral inhibition circuit (LIC), synapse control circuit (SCC), dual switch control circuit (DCC), and update control circuit (UCC). The arrows indicate the flow of signals among these components. The working of memristive SNN are as follows:

- The input feature vector \mathbf{x} is pre-processed and then converted into *pre_spikes* using a temporal spike encoder.
- These spikes are sent to the dual switches, dual switch control circuits, and update control circuits.
- The dual switches transmit either *pre_spikes* or synapse update voltages (v_{updt}) to the MC, depending on the control signal $\overline{v_s}$.
- Within the MC, two primary operations take place: the production of weighted spike currents and the modification of synaptic weights (conductance of memristors).
- The LIF neurons receive these weighted spike currents to generate a *post_spike*.
- This *post_spike* is then sent to both the LIC and SCC modules.
- In response to the *post_spike*, the LIC generates signals v_{inh} and $v_{C_{inh}}$.
- The UCC utilizes $v_{C_{inh}}$ to produce v_{updt} .
- The v_{inh} signal is forwarded to the LIF neurons, SCC, and DCC to perform lateral inhibition and establish a refractory period, generating v_e , and $\overline{v_s}$, respectively. The

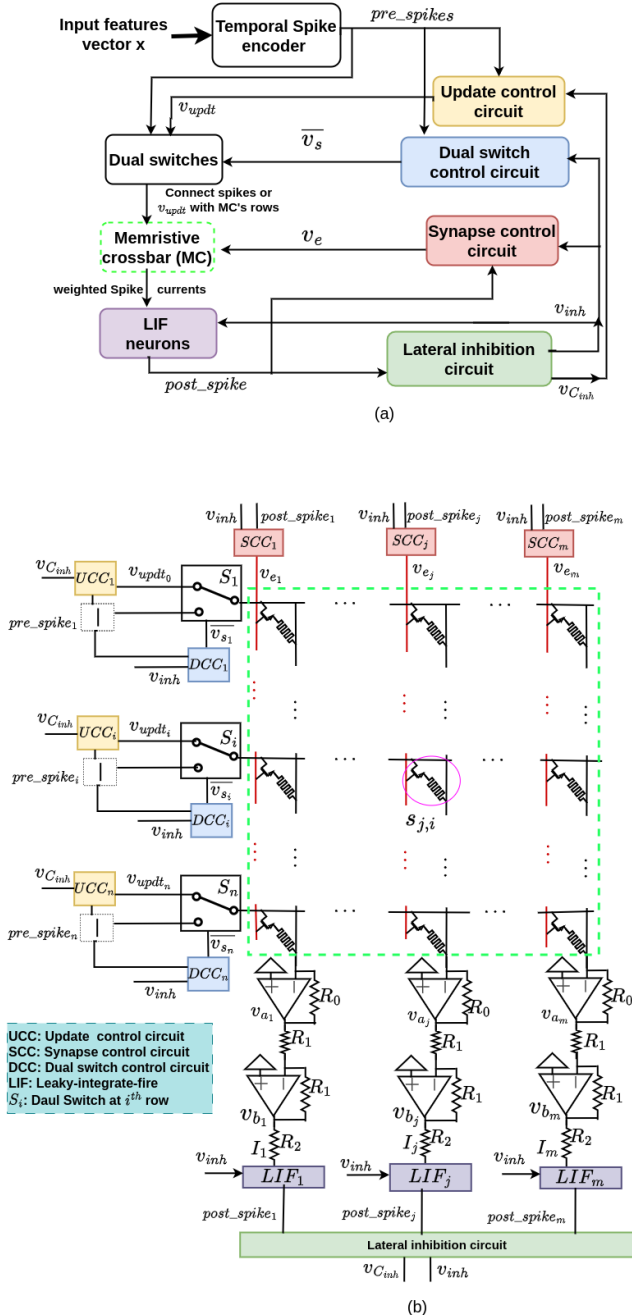


Fig. 2. (a) Overview of the memristive SNN architecture. The arrows indicate the information flow. (b) Architectural layout of the memristive SNN. Switch S_i enables pre_spike_i on the i^{th} row. The pre_spike_i reaches post-neuron LIF_j via synapse $s_{j,i}$ to contribute to integration and fire activities.

v_e and \bar{v}_s signals regulate the synapses and dual switches respectively.

The layout of the memristive SNN architecture is shown in Fig. 2(b). For a dataset with n features and m classes, it requires a 1T1M memristor crossbar of size $n \times m$, as indicated by the dashed green box in Fig. 2(b). This setup includes n pre-spikes, one for each feature, and m post-neurons correspond to m classes. Each i^{th} row in the crossbar is associated with an Update Control Circuit (UCC_i), a Dual Switch Control Circuit (DCC_i), and a dual switch S_i . The j^{th} column has a Synapse Control Circuit (SCC_j) at the top and two operational

amplifiers (Opamps) and a Leaky Integrate-and-Fire neuron (LIF_j) at the bottom. All LIF neurons are connected to a lateral inhibition circuit.

With this overview and architectural layout, we describe each component and their functionalities illustrating spice simulations of a memristive SNN with 12 pre-spikes and three post-neurons.

A. Temporal Spike Encoder

The inputs to the memristive SNN are spikes. Therefore, each element x_i of vector x is encoded into spikes and spread into time sequence length T . The temporal spike encoder is a functional block that converts x_i into pre_spike_i . In this work, the temporal spike encoding scheme is used where pre_spike_i corresponding to feature x_i arrives to post neurons at the moment $(T - x_i)$ [8], [38].

For simulation, the pre-spikes are represented with triangular pulses with $1\mu Sec$ rise and fall times. The height of pre-spikes is $1.1 V$ within memristors' thresholds. The simulated pre-spikes are presented in Figs. 4(a). The pre_spike_i is given to dual switch S_i to pass it to the i^{th} row of MC.

B. Dual Switches

As shown in Fig. 2(b), the i^{th} row of MC is associated with a dual switch S_i . The S_i either allows the update voltage v_{updt_i} from UCC_i or the pre_spike_i to the i^{th} row, depending on the switch control signal \bar{v}_{s_i} coming from DCC_i . These voltage-controlled dual switches may be designed in the Spice simulator [7].

C. Memristive Crossbar

The memristive crossbar employed here is of 1T1M type as shown in Fig. 2(b), green dashed box. There are n rows and m columns corresponding to the number of pre_spikes and output neurons, respectively. Each artificial synapse $s_{j,i}$ connecting i^{th} row and j^{th} column, as shown in the pink circle in Fig. 2(b), consists of one transistor and one memristor. The synapses of j^{th} column are made active or inactive by synapse control voltage v_{e_j} from SCC_j . The MC represents the synaptic weight matrix where conductance $G_{j,i}$ of memristor $M_{j,i}$ representing weight $w_{j,i}$ of synapse $s_{j,i}$ between pre_spike_i and post-neuron LIF_j is a matrix element. On arriving of pre_spike_i at $s_{j,i}$, it produces a weighted spike current proportional to $G_{j,i}$. The j^{th} column with the conjunction of two operational amplifiers outputs current I_j proportional to the sum of spike currents of synapses $s_{j,i}$, where $i = 1$ to n . The current I_j is passed to LIF_j to fire the $post_spike_j$.

D. Leaky-Integrate-Fire Neuron

Fig. 3 shows the proposed LIF neuron schematic. It consists of membrane capacitor C_m , leaking resistor R , resting potential v_{rest} , and two voltage-controlled switches named S_{inh} and S_{spk} controlled by v_{inh} and v_{spk} respectively. The spike current I_j coming from column j of MC is integrated across C_m in this LIF_j circuit. The v_{C_m} increases gradually because of this integration. The Opamp compares threshold potential

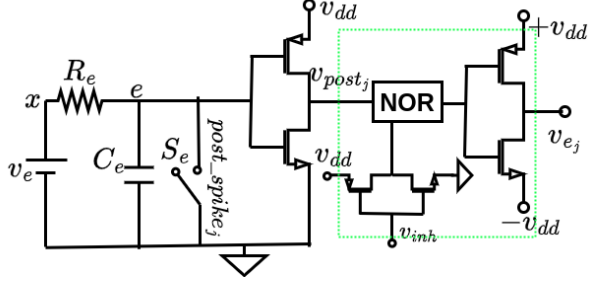


Fig. 6. The schematic of the synapse control circuit. The circuit parameters: $v_e = 5V$, $R_e = 1k\Omega$, $C_e = 1.7\mu F$, $v_{dd} = 5V$, $+v_{dd} = 5V$, $-v_{dd} = -5V$, and threshold of switch S_e is $0.4V$.

first case, all synapses are active whereas in the second case, only the synapses of the winner neuron are active and the rest are inactive. Supporting the above logic, the synapse control circuit (SCC) of LIF_j in Fig. 6 generates voltage signal v_{ej} . The v_{ej} turns T ON or OFF of all synapses of LIF_j if it is at peak or base voltage levels respectively. In other words, the amplitude of v_{ek} , for all $k = 1$ to m , is high before the winner's post-spike and thereafter only v_{ej} is at peak if LIF_j is the winner.

Initially, the capacitor C_e is fully charged, and the voltage v_{post_j} is low. When $post_spike_j$ occurs, S_e closes, C_e discharges, and the amplitude of v_{post_j} becomes high. The signal v_{ej} remains low only if LIF_j has not spiked while any other LIF neuron has. This behavior of v_{ej} corresponds to the logical operation $\overline{v_{ej}} = \overline{v_{post_j}} \wedge v_{inh}$, where v_{inh} is the inhibition signal. The green dotted section of the schematic in Fig. 6 implements this logic. For all non-winner neurons LIF_k , the amplitude of v_{ek} is at low level turning the synapses connected to LIF_k OFF, thereby preventing unwanted weight modification. The NOR block in this work is implemented with MOSFET transistors.

In Fig. 4(e), all v_{e1} , v_{e2} , and v_{e3} are high before post spikes in Fig. 4(c) but after $post_spike_2$ and $post_spike_3$ only v_{e2} and v_{e3} are continued to be high till the width of v_{inh} .

G. Dual Switch Control Circuit

Either pre_spike_i or voltage v_{updt_i} is allowed to i^{th} row of MC at a time by dual switch S_i (refer Fig. 2(b)). The v_{updt_i} updates active synapse of row i . This S_i is controlled by voltage $\overline{v_{s_i}}$ coming from the DCC_i , shown in Fig. 7, present at i^{th} row. When $\overline{v_{s_i}}$ is at peak then S_i allows pre_spike_i else v_{updt_i} . When both pre_spike_i has occurred and the winner post-neuron LIF_j has fired a $post_spike_j$, not necessarily at the same time, then only the S_i connects v_{updt_i} to the i^{th} row of the MC to update memristor $M_{j,i}$ otherwise it allows pre_spike_i .

In Fig. 7, the switch S_w is controlled by pre_spike_i . When pre_spike_i occurs, it turns S_w ON, discharging capacitor C_w and raising v_{pre_i} . When both v_{pre_i} and v_{inh} are at high then this indicates the occurrence of pre_spike_i and the post-spike of the winner neuron respectively. Consequently, the circuit generates a low (base) voltage $\overline{v_{s_i}}$, signaling the start of synaptic weight update. The time duration till $\overline{v_{s_i}}$ is low

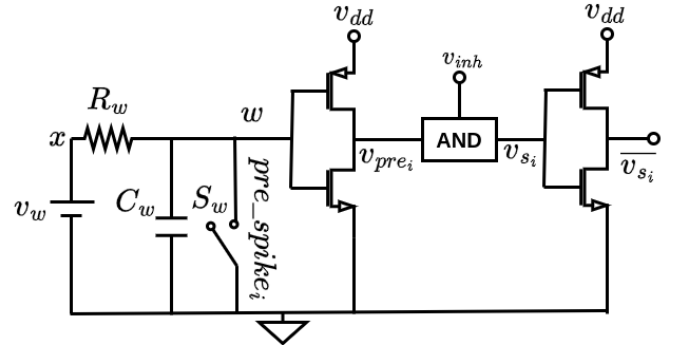


Fig. 7. The dual switch control circuit. The circuit parameters: $v_w = 5V$, $C_w = 1.5\mu F$, $R_w = 1k\Omega$, $v_{dd} = V$, and threshold of switch S_w is $1.1V$.

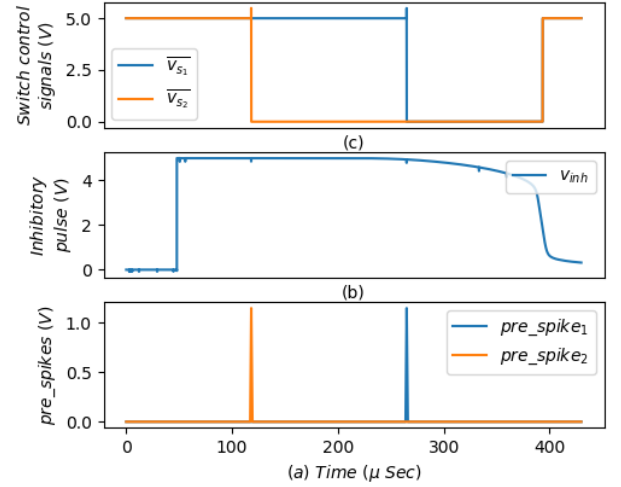


Fig. 8. (a) The features encoded into pre_spikes . (b) The start of inhibition pulse v_{inh} from LIC in Fig. 5 indicates the occurrence of winner $post_spike_j$. (c) The $\overline{v_{s_i}}$ allows the v_{updt_i} to modify synapse $s_{j,i}$ when it is low. The amplitude of $\overline{v_{s_i}}$ is low i.e., the $s_{j,i}$ is updated, only when both pre_spike_i and $post_spike_j$ have occurred.

denotes the update period of synapses $s_{j,i}$ of the winner neuron, LIF_j . The AND block is implemented with MOSFET transistors.

The spice simulation results of DCCs of row_1 and row_2 are illustrated in Figs. 8(a) to (c). In Fig. 8(a) two pre-spikes at row_1 and row_2 are occurred. When the v_{inh} becomes high in Fig. 8(b) it indicates the timing of the occurrence of post-spike. In Fig. 8(c), the $\overline{v_{s_1}}$ and $\overline{v_{s_2}}$ are low when winner neuron fired the post-spike and two pre-spikes (pre_spike_1 and pre_spike_2) have occurred. Therefore, the v_{updt_1} and v_{updt_2} are allowed by S_1 and S_2 to row_1 and row_2 till the $\overline{v_{s_1}}$ and $\overline{v_{s_2}}$ are low respectively.

H. Update Control Circuit

The conductance of the memristor in an active synapse is increased or decreased by applying positive or negative voltages across it, respectively. For a synapse $s_{j,i}$, the synaptic weight i.e., conductance $G_{j,i}$ is increased if pre_spike_i occurs before $post_spike_j$ and vice-versa. The UCC in Fig. 9 produces v_{updt_i} to modify the $G_{j,i}$ depending on the temporal order of occurring of these spikes. In order to increase $G_{j,i}$

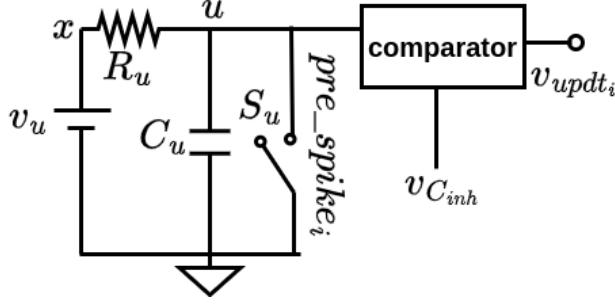


Fig. 9. The schematic of the update control circuit. The circuit parameters: $v_u = 5V$, $C_u = 1.5\mu F$, $R_u = 1k\Omega$, threshold of $S_u = 1.1$. if $v_{C_u} > v_{C_{inh}}$ then $v_{updt_i} = 1.4V$ else $v_{updt_i} = -2.6V$.

of memristor $M_{j,i}$ in synapse $s_{j,i}$, the voltage v_{updt_i} must be positive and greater than the memristor's threshold voltage. Conversely, to decrease $G_{j,i}$, the opposite conditions must hold. In the LIC schematic in Fig. 5, the C_{inh} is discharged by the winner's post-spike, and in Fig. 9 C_u is discharged by pre_spike_i . These capacitors are recharged by v_l and v_u respectively where $v_l = v_u$ and $C_{inh} = C_u$. By comparing the voltages $v_{C_{inh}}$ and v_{C_u} across C_{inh} and C_u respectively, the order of occurrence of pre_spike_i and $post_spike_j$ is predicted. The comparator compares $v_{C_{inh}}$ with v_{C_u} to produce v_{updt_i} . If pre_spike_i occurs before $post_spike_j$, then $v_{C_u} > v_{C_{inh}}$, resulting in a positive v_{updt_i} . Conversely, if pre_spike_i occurs after $post_spike_j$, then $v_{C_u} < v_{C_{inh}}$, and v_{updt_i} is negative.

The simulated outputs of UCC are shown in Figs. 10(a) to (c). In Fig. 10(a), pre_spike_1 and pre_spike_2 occurred before and after $post_spike_2$ in Fig. 10(b). The v_{updt_1} and v_{updt_2} are produced by UCC_1 and UCC_2 respectively, in Fig. 10(c). In the proposed model, a synapse starts updating its weight only when both pre- and post-spikes have occurred. Therefore, for the synapse $s_{j,i}$ the value of v_{updt_i} is considered effective only when pre_spike_i and $post_spike_j$ have occurred.

IV. SUPERVISED IN-SITU STDP TRAINING

The memristive SNN is trained using the proposed hardware-friendly supervised in-situ STDP algorithm. The in-situ training is capable of mitigating any hardware imperfections present in devices [42] as well as it is more energy-efficient and faster due to reduced communication with external hardware [25]. The dataset is divided into training and test sets. Training is performed with the training set while testing is done over the test set. The input features are converted into spikes as explained in Sections III-A. The training involves iteratively presenting input spikes from the training set to the memristive SNN using the procedure outlined in algorithm 1. Here the data sample's label supervises the training procedure.

According to STDP rules for synapse $s_{j,i}$, if the pre_spike_i occurs before the $post_spike_j$, the conductance $G_{j,i}$ ($\equiv w_{j,i}$) of the memristor $M_{j,i}$ increases and vice-versa. The magnitude of the conductance change decreases with the increase in time difference between these spikes.

Initially, all memristors in the MC are set to a high conductance state G_{max} . For an input with label j , only

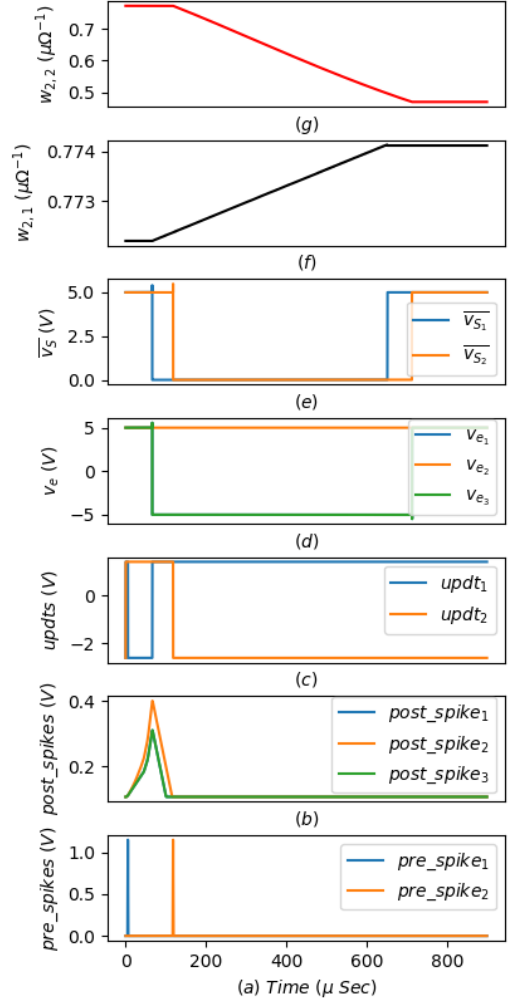


Fig. 10. The plots (a) to (g) are to explain training steps. (a) pre-spikes. (b) LIF_2 is winner firing $post_spike_2$. (c) Update voltages in rows 1 and 2. (d) Only v_{e2} is high during the update making synapses of LIF_2 active. (e) The update windows for synapses $s_{2,1}$ and $s_{2,2}$ are decided by \bar{v}_{s1} and \bar{v}_{s2} being low. The weights $w_{2,1}$ and $w_{2,2}$ in plots (f) and (g) increased and decreased following the orders of pre- and post-spikes.

LIF_j receives an extra bias current I_{b_j} to achieve supervised training. The I_{b_j} should be large enough to make LIF_j winner. The synaptic weight update begins when $post_spike_j$ occurs. If synapse $s_{j,i}$ is ON (i.e., the amplitude of v_{e_j} is high) and the update voltage v_{updt_i} is applied to row i by making \bar{v}_{s_i} low, then the memristor $M_{j,i}$ receives the v_{updt_i} across it that results in modification in $G_{j,i}$ depending on the sign and magnitude of v_{updt_i} . All the synaptic weights of winner neurons are updated parallel. The update rules are detailed in Table III. The same algorithm 1 is used for both, binary pattern recognition and input vector classification problems.

TABLE III
UPDATE RULES FOR SYNAPSE $s_{j,i}$. *: DON'T CARE

\bar{v}_{s_i}	v_{e_j}	pre_spike_i	$post_spike_j$	Weight $G_{j,i}$
High	*	*	*	No change
*	Low	*	*	No change
Low	High	Before	After	↑
Low	High	After	Before	↓

Algorithm 1: Supervised In-situ STDP Training.

Data: Temporal encoded spikes corresponding to input vector \mathbf{x} with label j ;

Result: The proper weight adjustment of all synapses of winner LIF_j ;

- 1 Make all synapses in the MC ON;
 - 2 Allow pre_spike_i corresponding to x_i , the i^{th} feature of input \mathbf{x} , to UCC_i , DCC_i , and dual switch S_i where $i = 1$ to n ;
 - 3 Apply an extra bias current I_{b_j} only to LIF_j , ensuring supervised training;
 - 4 LIF_j fires $post_spike_j$ first due to the sufficient bias current I_{b_j} ;
 - 5 The $post_spike_j$ is input to lateral inhibition circuit and all SCCs;
 - 6 The $post_spike_j$ causes lateral inhibition circuit to output inhibitory pulse v_{inh} and voltage $v_{C_{inh}}$ across capacitor C_{inh} in this circuit;
 - 7 The v_{inh} is input to all LIFs, DCCs, and SCCs ;
 - 8 The $v_{C_{inh}}$ is input to all UCCs;
 - 9 The v_{inh} inhibits all LIF neurons from firing except LIF_j , making LIF_j the winner;
 - 10 SCC_j makes all the synapses ON connected to LIF_j while those connected to other neurons OFF;
 - 11 Switch S_i connects row i of MC to v_{updt_i} from UCC_i during update time window;
 - 12 Update $G_{j,i}$ of memristor $M_{j,i}$ in synapse $s_{j,i}$ based on whether v_{updt_i} is positive (increase) or negative (decrease).
-

1) *Pattern Recognition:* The labeled binary patterns of size $r \times c$, where r and c are the numbers of rows and columns respectively, are encoded into spikes using temporal encoding. The bits of binary patterns are encoded row-wise into spikes and given to the memristive SNN for training using algorithm 1. Here no pre-processing is required. The examples of 5×3 binary patterns are shown in Fig. 11(a).

2) *Classification Problem:* In classification problems, the pre-processing of inputs with the Gaussian receptive field method is done to smooth the population of spikes as explained in Section II-C. After pre-processing of input vectors, they are encoded into spikes and given to algorithm 1.

A. Testing Phase

During the testing phase, all synapses are ON, and pre-synaptic spikes corresponding to the input are applied to the rows of the MC. In this phase, synaptic weights are not updated. The recognition or classification of input \mathbf{x} with label j is said to be correct if and only if LIF_j fires a spike.

V. SIMULATION AND RESULTS

The functioning of the memristive SNN and in-situ training Algorithm 1 is verified by simulating them using LTspice simulator running on an Ubuntu 20.04 LTS environment with an 8-core 1.6GHz Intel Core i5 processor and 8GB RAM. Its functionality is verified for pattern recognition and

TABLE IV
NETWORK PARAMETERS

Dataset	# feature (n) or pre-spikes after pre-processing	# classes (m) or post-spikes	MC size # synapses	R_0 (Ω)	R_1 (Ω)	R_2 (Ω)	C_m	I_b
IRIS	12	3	36	95k	1k	500	5 μ F	35 μ A
BCW	90	2	180	40k	1k	500	7 μ F	100 μ A
5×3	15, no pre-processing	4	60	30k	1k	1k	0.3 μ F	500 μ A

vector classification tasks. The simulations are performed to recognize binary images in Fig. 11(a) and to classify labeled datasets like IRIS [43] and Breast Cancer Wisconsin (BCW) [43]. For different data sets, the network structure and parameters are shown in Table IV. The simulation employs the memristor model described by [29] with positive and negative thresholds as 1.2V and $-2.4V$, respectively. The positive and negative values of update voltage v_{updt} are 1.4V and $-2.6V$, respectively. The pre-spikes are triangular pulses with 1 μ s rise and fall times, and amplitude of 1.1V. The memristor's minimum conductance $G_{min} = 0.0167 \mu\Omega^{-1}$ and maximum conductance $G_{max} = 1 \mu\Omega^{-1}$.

Fig. 10 illustrates the intermediate simulation results of the training of the memristive SNN. Figs. 10(a) to (g) brief the synaptic plasticity process during the training of the memristive SNN. In Fig. 10(a), pre_spike_1 and pre_spike_2 occur before and after $post_spike_2$ of winner LIF_2 , in Fig. 10(b), respectively. In Fig. 10(c), the update voltages v_{updt_1} and v_{updt_2} from UCC_1 and UCC_2 are shown. Accordingly, only v_{e_2} are high making all synapses of LIF_2 active and rest of the synapses are inactive as v_{e_1} and v_{e_3} are low, refer Fig. 10(d). When both pre and post-spikes have occurred then only $\overline{v_{s_1}}$ and $\overline{v_{s_2}}$ are low, in Fig. 10(e), that means the update voltages v_{updt_1} and v_{updt_2} are fed to row_1 and row_2 to MC respectively. In Figs. 10(f) and (g) following the update rules in Table III, the weights $w_{2,1}$ and $w_{2,2}$ are adjusted based on the temporal ordering of $pre_spike_1 - post_spike_2$ and $pre_spike_2 - post_spike_2$. This demonstrates the correctness of the proposed training method.

A. Simulation for pattern recognition

The four binary patterns of size 5×3 labeled 0, 1, 2, and 3 are chosen to train the memristive SNN, as shown in Fig. 11(a). There are 15 pre-neurons and four post-neurons. Temporal spike encoding is used to map the pixels into pre-spikes, where a pre-spike corresponding to a black pixel occurs 0.5 ms before than that of the white pixel. The training set comprises 100 samples (patterns 0, 1, 2, and 3 with 25 each). After training, the memristive SNN recognizes all four patterns correctly in the testing phase. The final synaptic weights are visualized as a heat map in Fig. 11(b), demonstrating the consistency with the input patterns.

B. Robustness Against Noisy Patterns

For pattern recognition tasks, the robustness of our memristive SNN was evaluated by introducing noises in the patterns through pixel flips (black to white or white to black). Our approach demonstrated better noise resilience compared to previous literature [6], [7], [23], as shown in Table V.

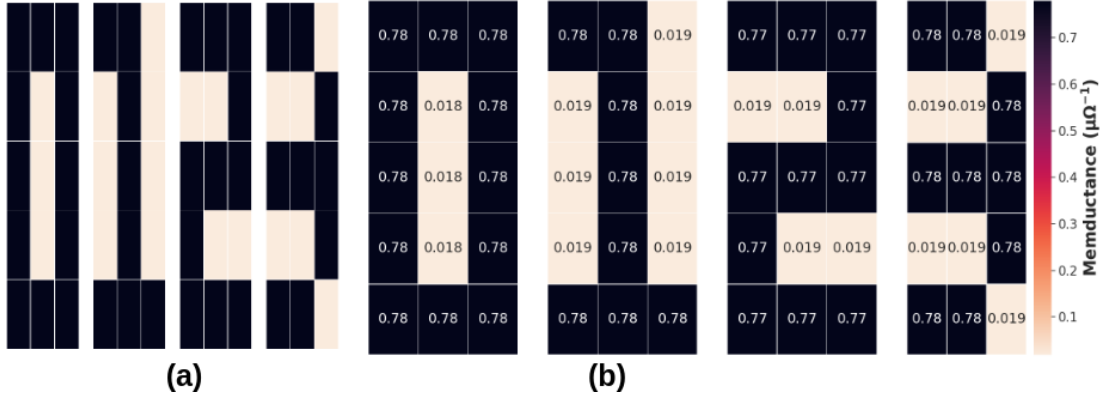


Fig. 11. (a) Binary training patterns, and (b) heat map of final synaptic weights in $\mu\Omega^{-1}$, which are consistent after training with the patterns used.

TABLE V
AVERAGE RECOGNITION ACCURACY UNDER DIFFERENT NOISE LEVELS.

Noise level	In [6]	In [7]	In [23]	In proposed work
noiseless	100%	100%	97.5%	100%
6.67%	96.67%	93.33%	—	100%
13.33%	87.46%	76.9%	—	95.47%
20%	—	—	—	93.4%

C. Scalability of the Memristive SNN architecture

The memristive SNN is scalable due to its modular architecture and can adapt to various pattern sizes and numbers. We illustrate this scalability by training the SNN with ten binary images (0 to 9) of size 7×3 with 21 pre- and 10 post-neurons. The heat map of the synaptic weights after training, presented in Fig. 12, agree with the patterns in the scaled memristive SNN. During testing, all patterns are recognized correctly.

D. Simulation for Classification

The inputs of the BCW and IRIS data sets are normalized first by Min-Max scaling, then pre-processed by applying Gaussian receptive fields [38] to increase the number of features three times. Originally, IRIS and BCW have 4 and 30 features, but they have increased to 12 and 90 after pre-processing, respectively. Therefore, the number of pre-spikes for IRIS and BCW are 12 and 90 respectively. The number of post-neurons or output neurons is three and two in the memristive SNN for IRIS and BCW, respectively. After training, we got the classification accuracy of 99.11% and 97.9% for the IRIS and BCW data sets, respectively. The comparison of F1-score and classification accuracies for IRIS and BCW with previous SNNs solving classification problems is presented in Table VI. The comparison shows, our memristive SNN gives better results. It is to note that in this work number of features increased by three times after pre-processing, but in work [8] same increases by twenty times.

E. Fault Analysis

The physical memristive crossbars are vulnerable to faults during fabrication in the foundry, which makes it relevant to study the effect of the non-ideal cases associated with memristors. The training of the memristive SNNs is simulated

to analyze the effect of the following three faults –(a) when memristors are stuck-at-a-conducting state, (b) when memristors have variations in their boundary resistances, and (c) when memristors' threshold has variations.

1) *Stuck-at-a-conductance state*: The physical memristor may be stuck at a conductance state and does not change its state even on the application of voltages greater than its threshold across it. We performed simulations for the IRIS and BCW datasets by choosing random 5%, 10%, and 20% of memristors that are stuck at random conducting states. With these faulty memristors, the training of memristive SNNs is performed with the algorithm 1 and results in the accuracies of 96.44%, 97.33%, and 92.88% for IRIS as well as 96.50%, 96.50%, and 96.50% for BCW data sets, respectively. The results demonstrate that the proposed architecture is robust against these faults. It is to be noted that the performance for the BCW data set does not change much because of its memristive SNN size compared to that of IRIS.

2) *Variations in boundary resistances R_{on} and R_{off}* : The random variations in the memristor's boundary resistance limits are added. The variation is defined by relative standard dispersion, i.e., the ratio between variation and mean value of the parameter [44]. The memristive SNN for IRIS data are trained by adding 5%, 10%, 20%, 25%, and 30% variations in the limits of both R_{on} and R_{off} of all memristors [29] of the MC and got 98.22%, 97.33%, 94.66%, 96%, and 81.34% accuracies respectively. The accuracies are evidence of the resilience of memristive SNN against these variations.

3) *Variations in memristor threshold voltages*: The memristor's threshold is very crucial for synaptic plasticity because the memristor's conductance is only changed if it experiences voltages greater than the threshold. The threshold parameters suffer from device-to-device variation. We analyzed this variation using the memristive SNN with the IRIS dataset. In order to consider this, we added 5% and 10% variations in positive and negative thresholds of all memristors of MC. After training, it gives 97.33% and 76.89% accuracies respectively. The results illustrate that the proposed model is sensitive to variations in the memristor's thresholds.

F. Discussion

The memristive SNNs circuits and in-situ algorithm together are a complete system that works without any separate control

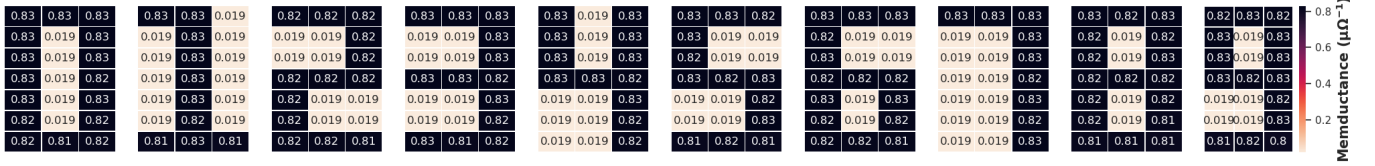


Fig. 12. In order to scale the SNN in terms of input and output neurons, ten binary digits 0 to 9 are taken to train. The final weights after training consist of digits 0 to 9 of size 7×3 .

TABLE VI
COMPARISON OF F1-SCORE AND CLASSIFICATION ACCURACY FOR DIFFERENT DATASETS WITH PREVIOUS WORKS.

Papers	F1-score		Accuracy		Memristive Architecture	Circuit level design	Simulated on Circuit
	IRIS	BCW	IRIS	BCW			
[38]	99%	90%	—	—	No	No	No
[8]	97%	90%	—	—	Yes	No	No
[9]	97.326%	—	97.33%	—	Yes	Yes	No
This work	98.68%	98.617%	99.11%	97.9%	Yes	Yes	Yes

unit like a micro-controller or FPGA, etc. The model is modular, scalable, and has shown great robustness against device variation, faulty memristors, and noisy patterns. From Table I, it is efficient in hardware complexity, which reduces area and energy consumption. For classification, the memristive SNNs with IRIS and BCW datasets took only 10 and 5 epochs to train them respectively with comparable accuracies, refer Table VI.

In this work, the threshold voltage of the NMOS transistor in 1T1M synapses is $0.5V$. The gate voltage is set to either $+5V$ or $-5V$ to switch the NMOS ON or OFF, respectively, resulting in the synapse being either active or inactive. At the drain terminal, we apply either a spike (maximum $1.1V$) or $1.4V$ or $-2.6V$. In these conditions, the NMOS synapse operates either in the cutoff or triode modes, but not in saturation. The total consumed power at a 1T1M synapse is the sum of the powers that NMOS and memristor consume individually. The power consumed by the NMOS transistor is the product of the drain current and the drain-source voltage when it is not in cut-off mode [45]. When the transistor is in the cut-off mode [46], no current passes through the NMOS transistor and memristor of the synapse, resulting in zero power consumption. Therefore, power is consumed only when the synapse is active and the NMOS transistor is in the triode mode. Through simulation, a synapse consumes, on average, $21.878\mu W$ of energy per input sample during training.

During the training of the memristive SNN for a pattern recognition task, it is observed that in the absence of bias current ($I_b = 0$) and with memristors randomly initialized near their low-resistance states, each output neuron becomes associated with a specific input pattern type, as illustrated in Fig. 13. This neuron-pattern association emerges in a random manner. The heat map shown in Fig. 13 indicates that $neuron_0$, $neuron_1$, $neuron_2$, and $neuron_3$ predominantly respond to $pattern_1$, $pattern_3$, $pattern_2$, and $pattern_0$, respectively. Notably, this process does not require label information during training, thereby demonstrating an unsupervised learning behavior.

As a continuation of this work, future efforts will investigate

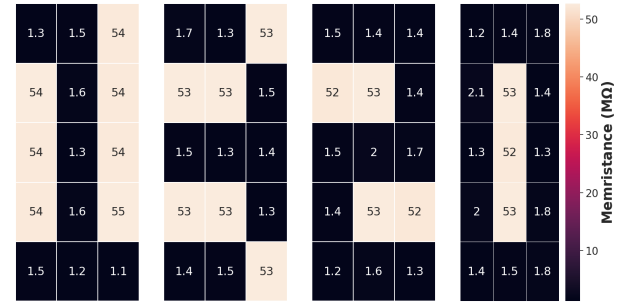


Fig. 13. Heat map of synaptic weights illustrating the association between output neurons and input pattern types after unsupervised training of the memristive SNN. Each neuron exhibits selective activation toward a distinct pattern despite the absence of supervision.

the detailed energy consumption characteristics of the proposed memristive SNN and explore its practical deployment in edge intelligent devices for larger datasets.

VI. CONCLUSION

In this work, we proposed a hardware-efficient memristive SNN architecture and an STDP-based supervised in-situ training algorithm to train it. It is robust against stuck-fault, device variation, and noisy input patterns. The lateral inhibition and refractory period concepts are efficiently employed in the architecture. The synapses of the winner neuron are modified concurrently. Its modularity makes it scalable. We got 99.11% and 97.9% classification accuracies for IRIS and Breast Cancer Wisconsin datasets, respectively. The memristive SNN gives 92.88% and 96.5% accuracies for IRIS and BCW, respectively when 20% randomly chosen memristors are stuck at random conducting states and do not change their states during training. The model gives 81.34% classification accuracy when memristors have 30% variations in their limit resistance values.

REFERENCES

- [1] O. I. Abiodun, A. Jantan, A. E. Omolara, K. V. Dada, N. A. Mohamed, and H. Arshad, "State-of-the-art in artificial neural network applications: A survey," *Heliyon*, vol. 4, no. 11, 2018.

- [2] K. Roy, A. Jaiswal, and P. Panda, "Towards spike-based machine intelligence with neuromorphic computing," *Nature*, vol. 575, no. 7784, pp. 607–617, 2019.
- [3] W. Maass, "Networks of spiking neurons: the third generation of neural network models," *Neural networks*, vol. 10, no. 9, pp. 1659–1671, 1997.
- [4] L. Zhao, Q. Hong, and X. Wang, "Novel designs of spiking neuron circuit and stdp learning circuit based on memristor," *Neurocomputing*, vol. 314, pp. 207–214, 2018.
- [5] X. Zhang, J. Lu, Z. Wang, R. Wang, J. Wei, T. Shi, C. Dou, Z. Wu, J. Zhu, D. Shang *et al.*, "Hybrid memristor-cmos neurons for in-situ learning in fully hardware memristive spiking neural networks," *Science Bulletin*, vol. 66, no. 16, pp. 1624–1633, 2021.
- [6] M. Li, X. Wang, and Z. Chen, "Fully circuit implementation of a two-layer memristive neural network for pattern recognition," in *ICIST*, 2021.
- [7] M. Li, Q. Hong, and X. Wang, "Memristor-based circuit implementation of competitive neural network based on online unsupervised hebbian learning rule for pattern recognition," *Neural Computing and Applications*, 2022.
- [8] A. G. Sboev, D. Vlasov, R. B. Rybka, Y. Davydov, A. Serenko, and V. A. Demin, "Modeling the dynamics of spiking networks with memristor-based stdp to solve classification tasks," *Mathematics*, 2021.
- [9] W. Jiang, J. Li, H. Liu, X. Qian, Y. Ge, L. Wang, and S. Duan, "Memristor-based multi-synaptic spiking neuron circuit for spiking neural network," *Chinese Physics B*, vol. 31, no. 4, p. 040702, 2022.
- [10] S. M. Bohte, J. N. Kok, and H. La Poutre, "Error-backpropagation in temporally encoded networks of spiking neurons," *Neurocomputing*, vol. 48, no. 1–4, pp. 17–37, 2002.
- [11] Y.-F. Liu, D.-W. Wang, Z.-K. Dong, H. Xie, and W.-S. Zhao, "Implementation of multiple-step quantized stdp based on novel memristive synapses," *IEEE Transactions on Very Large Scale Integration (VLSI) Systems*, vol. 32, no. 8, pp. 1369–1379, 2024.
- [12] J. S. Verma, P. Kumar, B. S. Makhdooni, R. K. Ranjan, and S.-M. Kang, "Memristor-emulator-based crossbar array for object detection and recognition," *IEEE Transactions on Circuits and Systems I: Regular Papers*, pp. 1–12, 2025.
- [13] D. B. Strukov, G. S. Snider, D. R. Stewart, and R. S. Williams, "The missing memristor found," *nature*, vol. 453, no. 7191, pp. 80–83, 2008.
- [14] L. Chua, "Memristor-the missing circuit element," *IEEE Transactions on Circuit Theory*, 1971.
- [15] W. Jiang, B. Xie, C.-C. Liu, and Y. Shi, "Integrating memristors and cmos for better ai," *Nature Electronics*, vol. 2, no. 9, pp. 376–377, 2019.
- [16] O. Mutlu, S. Ghose, J. Gómez-Luna, and R. Ausavarungnirun, "A modern primer on processing in memory," in *Emerging Computing: From Devices to Systems: Looking Beyond Moore and Von Neumann*, 2022, pp. 171–243.
- [17] W. A. Wulf and S. A. McKee, "Hitting the memory wall: Implications of the obvious," *ACM SIGARCH Computer Architecture News*, 1995.
- [18] G. Pedretti, V. Milo, S. Ambrogio, R. Carboni, S. Bianchi, A. Calderoni, N. Ramaswamy, A. Spinelli, and D. Ielmini, "Memristive neural network for on-line learning and tracking with brain-inspired spike timing dependent plasticity," *Scientific reports*, vol. 7, no. 1, p. 5288, 2017.
- [19] M. Hansen, F. Zahari, H. Kohlstedt, and M. Ziegler, "Unsupervised hebbian learning experimentally realized with analogue memristive crossbar arrays," *Scientific reports*, 2018.
- [20] Y. Jiang, P. Huang, D. Zhu, Z. Zhou, R. Han, L. Liu, X. Liu, and J. Kang, "Design and hardware implementation of neuromorphic systems with rram synapses and threshold-controlled neurons for pattern recognition," *IEEE Transactions on Circuits and Systems I: Regular Papers*, vol. 65, no. 9, pp. 2726–2738, 2018.
- [21] Z. Hajiabadi and M. Shalchian, "Memristor-based synaptic plasticity and unsupervised learning of spiking neural networks," *Journal of Computational Electronics*, vol. 20, no. 4, pp. 1625–1636, 2021.
- [22] D. Wang, J. Xu, F. Li, L. Zhang, C. Cao, D. Stathis, A. Lansner, A. Hemani, L.-R. Zheng, and Z. Zou, "A memristor-based learning engine for synaptic trace-based online learning," *IEEE Transactions on Biomedical Circuits and Systems*, vol. 17, no. 5, pp. 1153–1165, 2023.
- [23] P. Zhou, D.-U. Choi, J. K. Eshraghian, and S.-M. Kang, "A fully memristive spiking neural network with unsupervised learning," in *2022 IEEE International Symposium on Circuits and Systems (ISCAS)*, 2022, pp. 634–638.
- [24] P. Wijesinghe, A. Ankit, A. Sengupta, and K. Roy, "An all-memristor deep spiking neural computing system: A step toward realizing the low-power stochastic brain," *IEEE Transactions on Emerging Topics in Computational Intelligence*, vol. 2, no. 5, pp. 345–358, 2018.
- [25] F. Alibart, E. Zamanidoost, and D. B. Strukov, "Pattern classification by memristive crossbar circuits using ex situ and in situ training," *Nature Communications*, vol. 4, no. 1, pp. 1–7, 2013.
- [26] P. U. Diehl and M. Cook, "Unsupervised learning of digit recognition using spike-timing-dependent plasticity," *Frontiers in computational neuroscience*, vol. 9, p. 99, 2015.
- [27] W. M. K. Wulfram Gerstner, *Spiking Neuron Models*. Cambridge University Press, 2002.
- [28] B. Linares-Barranco and T. Serrano-Gotarredona, "Memristance can explain spike-time-dependent-plasticity in neural synapses," *Nature preceedings*, 2009.
- [29] Y. Zhang, X. Wang, Y. Li, and E. G. Friedman, "Memristive model for synaptic circuits," *IEEE Transactions on Circuits and Systems II: Express Briefs*, 2017.
- [30] A. M. Sheri, H. Hwang, M. Jeon, and B.-g. Lee, "Neuromorphic character recognition system with two pcmo memristors as a synapse," *IEEE Transactions on Industrial Electronics*, vol. 61, no. 6, pp. 2933–2941, 2014.
- [31] M. Chu, B. Kim, S. Park, H. Hwang, M. Jeon, B. H. Lee, and B.-G. Lee, "Neuromorphic hardware system for visual pattern recognition with memristor array and cmos neuron," *IEEE Transactions on Industrial Electronics*, vol. 62, no. 4, pp. 2410–2419, 2014.
- [32] C. Yakopcic, T. M. Taha, G. Subramanyam, R. E. Pino, and S. Rogers, "Analysis of a memristor based 1t1m crossbar architecture," in *The 2011 International Joint Conference on Neural Networks*, 2011.
- [33] R. Hasan, C. Yakopcic, and T. M. Taha, "Ex-situ training of large memristor crossbars for neural network applications," *Analog Integrated Circuits and Signal Processing*, vol. 99, pp. 1–10, 2019.
- [34] M. Teimoori, A. Amirsoleimani, A. Ahmadi, and M. Ahmadi, "A 2m1m crossbar architecture: Memory," *IEEE Transactions on Very Large Scale Integration (VLSI) Systems*, vol. 26, no. 12, pp. 2608–2618, 2018.
- [35] D. Soudry, D. Di Castro, A. Gal, A. Kolodny, and S. Kvatinsky, "Memristor-based multilayer neural networks with online gradient descent training," *IEEE transactions on neural networks and learning systems*, vol. 26, no. 10, pp. 2408–2421, 2015.
- [36] T.-H. Kim, S. Kim, J. Park, S. Youn, and H. Kim, "Memristor crossbar array with enhanced device yield for in-memory vector–matrix multiplication," *ACS Applied Electronic Materials*, vol. 6, no. 6, pp. 4099–4107, 2024.
- [37] M. Hu, J. P. Strachan, Z. Li, E. M. Grafals, N. Davila, C. Graves, S. Lam, N. Ge, J. J. Yang, and R. S. Williams, "Dot-product engine for neuromorphic computing: Programming 1t1m crossbar to accelerate matrix-vector multiplication," in *Proceedings of the 53rd annual design automation conference*, 2016, pp. 1–6.
- [38] A. Sboev, A. Serenko, R. Rybka, and D. Vlasov, "Solving a classification task by spiking neural network with stdp based on rate and temporal input encoding," *Mathematical Methods in the Applied Sciences*, vol. 43, no. 13, pp. 7802–7814, 2020.
- [39] J. Wang, A. Belatreche, L. Maguire, and T. M. McGinnity, "An online supervised learning method for spiking neural networks with adaptive structure," *Neurocomputing*, vol. 144, pp. 526–536, 2014.
- [40] Q. Yu, H. Tang, K. C. Tan, and H. Yu, "A brain-inspired spiking neural network model with temporal encoding and learning," *Neurocomputing*, vol. 138, pp. 3–13, 2014.
- [41] R. Gütiğ and H. Sompolsky, "The tempotron: a neuron that learns spike timing-based decisions," *Nature neuroscience*, vol. 9, no. 3, pp. 420–428, 2006.
- [42] C. Li, D. Belkin, Y. Li *et al.*, "Efficient and self-adaptive in-situ learning in multilayer memristor neural networks," *Nature Communications*, vol. 9, no. 1, p. 2385, 2018.
- [43] D. Dua and C. Graff, "UCI machine learning repository," 2017. [Online]. Available: <http://archive.ics.uci.edu/ml>
- [44] Z. Zhao, L. Qu, L. Wang, Q. Deng, N. Li, Z. Kang, S. Guo, and W. Xu, "A memristor-based spiking neural network with high scalability and learning efficiency," *IEEE Transactions on Circuits and Systems II: Express Briefs*, vol. 67, no. 5, pp. 931–935, 2020.
- [45] N. H. Weste and D. Harris, *CMOS VLSI design: a circuits and systems perspective*. Pearson Education India, 2015.
- [46] J. Wang, "Mosfets power consumption and power dissipation calculation," in *Journal of Physics: Conference Series*, vol. 1754, no. 1. IOP Publishing, 2021, p. 012132.